Lifetime measurements of the yrast 8^{+} and 9^{+} states in ^{70}As

C. Morse, H. Iwasaki, A. Lemasson, T. Baugher, D. Bazin, J. S. Berryman, A. Dewald, C. Fransen, A. Gade, S. McDaniel, A. J. Nichols, A. Ratkiewicz, S. R. Stroberg, P. Voss, R. Wadsworth, D. Weisshaar, K. Wimmer, and R. Winkler

Phys. Rev. C **90**, 034310 — Published 15 September 2014

DOI: 10.1103/PhysRevC.90.034310

Lifetime measurements of the yrast 8^+ and 9^+ states in ^{70}As

C. Morse,[1,2] H. Iwasaki,[1,2] A. Lemasson,[1] T. Baugher,[1,2] D. Bazin,[1] J.S. Berryman,[1]
A. Dewald,[3] C. Fransen,[3] A. Gade,[1,2] S. McDaniel,[1,2] A.J. Nichols,[4] A. Ratkiewicz,[1,2]
S.R. Stroberg,[1,2] P. Voss,[1,2,5] R. Wadsworth,[4] D. Weisshaar,[1] K. Wimmer,[1] and R. Winkler[1]

[1]*National Superconducting Cyclotron Laboratory, Michigan State University, East Lansing, Michigan 48824, USA*
[2]*Department of Physics and Astronomy, Michigan State University, East Lansing, Michigan 48824, USA*
[3]*Institut für Kernphysik der Universität zu Köln, D-50937 Köln, Germany*
[4]*Department of Physics, University of York, Heslington, York YO10 5DD, United Kingdom*
[5]*Department of Chemistry, Simon Fraser University, Burnaby, British Columbia, V5A 1S6 Canada*

(Dated: July 8, 2014)

The lifetimes of the yrast 8^+ and 9^+ states of ^{70}As have been measured via the γ-ray lineshape method following population by the ^{9}Be(^{78}Rb,^{70}As) reaction at 101.6 MeV/nucleon. The strength of the E1 $8^+ \rightarrow 7^-$ transition is found to be $B(E1) = 1.3(5) \times 10^{-5}$ e^2fm^2 or $1.2(4) \times 10^{-5}$ Weisskopf units (W.u.) while the $9^+ \rightarrow 8^+$ M1 transition is found to have a strength of $B(M1) = 1.5(8)$ μ_N^2 or 0.85(42) W.u. The implications for the structure of these states is discussed and found to be consistent with an assignment to a $\pi g_{9/2} \nu g_{9/2}$ configuration.

PACS numbers: 21.10.Tg, 21.10.Re, 25.60.-t, 27.50.+e

I. INTRODUCTION

Nuclei in the $A \sim 70$, $Z \sim 34$ region of the nuclear chart are known to be the site of a diverse set of structural phenomena [1]. As a function of nucleon number, many nuclei in this region evolve through a range of collectivity and nuclear shapes, including nearly spherical, prolate, and oblate, and with varying degrees of triaxiality. In addition, multiple shapes may coexist within the same nucleus, with different configurations competing to become the yrast configuration [2].

The evolution of the structure of the $A \sim 70$, $Z \sim 34$ nuclei is not constrained to vary only with changes in nucleon number but may also evolve with increasing excitation energy and angular momentum. Especially for $A \lesssim 70$ nuclei which are located in the lighter area of this mass region, low-lying excited states may be expected to be well-described by nucleons that occupy primarily the p and f shell-model orbitals. At higher excitation energies, however, these nuclei may be expected to show evidence for increasing occupation of the $g_{9/2}$ intruder orbital in the structure of the nuclear states [3].

Odd-odd nuclei offer a unique opportunity to study the effects of the occupation of intruder orbitals by valence nucleons. In the absence of collectivity, the states of an odd-odd nucleus of mass A can be constructed from the coupling of the odd proton and odd neutron into angular momentum multiplets coupled to the $(A-2)$ even-even core. In such a picture, transitions between excited states in the nucleus should have a strong single-particle character, as it is only the odd particles which participate in the transitions. Conversely, it is well-known that the $g_{9/2}$ configuration is considered to be responsible for driving deformation and collectivity in this region of the nuclear chart [4], and so one might expect that, upon occupation of the $g_{9/2}$ orbital by either or both of the uncoupled nucleons, the excited states would display a collective rather than single-particle nature. The study of states in which these nucleons occupy the $g_{9/2}$ orbital can therefore provide valuable insight into the effects of intruder configurations on nuclear structure.

In order to investigate the effects of occupying such high-lying intruder configurations, we have studied the odd-odd nucleus $^{70}_{33}$As$_{37}$. We have measured for the first time the lifetimes of the yrast 8^+ and 9^+ states in this nucleus and deduced the reduced transition strengths $B(E1; 8^+ \rightarrow 7^-)$ and $B(M1; 9^+ \rightarrow 8^+)$. Previous studies [5, 6] have suggested that the parent states in these transitions can be described well by the coupling of the odd proton and odd neutron in the configuration where they both occupy the $g_{9/2}$ orbital (denoted $\pi g_{9/2} \nu g_{9/2}$ hereafter). These assignments were based on arguments stemming from the correlation of the 9^+ energy with the sum of the $\frac{9}{2}^+$ state energies in the neighboring odd-A nuclei [5, 6] and the strong M1 branch connecting the 9^+ and the 8^+ states [6]. These studies also suggest that there is a decoupled band [7] built on the 9^+ state, specifically consisting of the 9^+, 11^+, and possibly the (13^+) states, which indicates that these states may have a collective nature. By contrast, the low-lying states of ^{70}As have been found to be well-described by a nearly spherical shape when the odd nucleons are not both in the $g_{9/2}$ orbital [6], and earlier work did not find any collective features among the low-lying states [5]. The new lifetime data in this work provide further insight into the nature of the higher-lying states and the possibility that the ^{70}As nucleus evolves collective features at moderate excitation energy.

Odd-odd nuclei present a challenging proposition for experimental studies. In this work, we use the γ-ray lineshape method [8, 9] in combination with a simulation package [10] to measure the lifetime of the 8^+ and 9^+ states in ^{70}As, which were populated using a multiple-nucleon removal reaction from a rare isotope beam of

^{78}Rb in order to excite levels with high angular momentum. The γ-ray lineshape provides an efficient way to measure the lifetimes of excited states of nuclei produced in rare isotope beams, especially those in the range of several tens to hundreds of picoseconds. In particular, it provides an alternative to the Recoil Distance Doppler Shift (RDDS) technique [11] when the production rate of the nucleus of interest is insufficient for an RDDS measurement. However, the level schemes of odd-odd nuclei are typically dense such that the identification of individual γ-rays can be difficult. In addition, higher-lying states may have lifetimes which are sizeable compared to those of the states of interest such that their feeding contribution may introduce systematic biases in the measurement. In order to circumvent these issues, the lineshape method was used with $\gamma\gamma$ coincidence data to control possible feeding effects and reduce contamination from other coincident γ-rays.

II. EXPERIMENT

The experiment was performed at the National Superconducting Cyclotron Laboratory at Michigan State University. A primary beam of ^{78}Kr was accelerated to 150 MeV/nucleon in the Coupled Cyclotron Facility and impinged on a ^{9}Be target to produce ^{78}Rb via nuclear charge exchange. The A1900 fragment separator [12] was used with an aluminum degrader to purify the secondary beam at a setting of 0.5% momentum acceptance. The resulting beam was composed of approximately 70% ^{78}Rb at 101.6 MeV/nucleon at an average rate of 1×10^5 pps. This secondary beam was transported to the experimental area where secondary reactions were induced on a 376 mg/cm^2 ^{9}Be target to produce ^{70}As. The reaction residues were identified according to the time-of-flight and energy-loss measured in the focal plane of the S800 spectrometer [13].

The γ-rays from the deexcitation of reaction products were detected with 15 HPGe detectors from the Segmented Germanium Array (SeGA) [14]. The array was deployed in a barrel configuration composed of two rings, one with eight detectors covering backward angles from 95°-125° and the other with seven detectors covering forward angles from 50°-80° with respect to the beam axis. This detector configuration was chosen in order to achieve both a high γ-ray detection efficiency (7.4% at 1 MeV for γ-ray singles events and 0.5% for 1 MeV $\gamma\gamma$ coincidence) and to maximize the sensitivity of the shape of the γ-ray spectrum to the lifetime of the excited states. The resulting γ-ray spectra, split into backward and forward angles and detected in coincidence with ^{70}As residues in the S800, are shown in Figs. 1(a) and (b), respectively. The energies of several prominent γ-rays observed in these spectra are labeled as candidates to explain the features of the spectrum. The 788.3 keV $8^+ \rightarrow 7^-$ transition can be clearly seen in both rings, as well as γ-ray peaks which may be explained by the 301.8 keV $2_1^- \rightarrow 1_1^+$ and the 474.12 keV $3_4^+ \rightarrow 2_2^+$ [15] transitions. On the other hand, there is a peak below 100 keV that is only visible in the backward ring. This discrepancy is due to the detection threshold on the forward ring being increased during the experiment to reduce the rate of photons being detected to a manageable level. The peak in the backward ring can be explained as originating from a combination of the 76.1 keV $9^+ \rightarrow 8^+$ transition and a contribution from radiative electron capture (REC) [16, 17] in the target which will be discussed in more detail later.

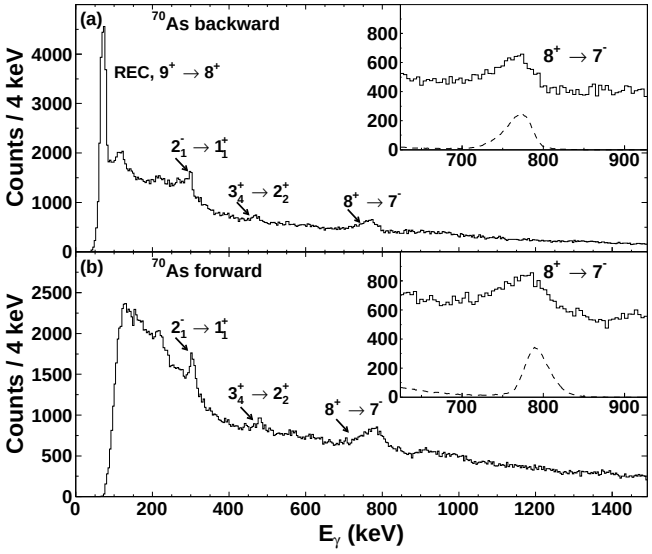

FIG. 1. Doppler-corrected γ-ray spectra obtained in coincidence with ^{70}As fragments detected in the S800 for (a) the backward detectors and (b) the forward detectors, along with candidates for the most prominent γ-rays observed in these spectra. The insets show a closer view of the $8^+ \rightarrow 7^-$ transition and the asymmetry in the associated 788.3 keV γ-ray peak due to the lifetime of the 8^+ state. Also pictured in the insets is a simulation assuming a lifetime $\tau_{8^+} = 0$ ps (dashed line). Comparison between the simulated backward and forward spectra shows that the backward spectrum already has a significant low-energy tail even with $\tau_{8^+} = 0$ ps because of decays happening at different velocities inside the target, and so will not be as sensitive as the forward detectors to the lifetime.

The lifetimes of the 8^+ and 9^+ states in ^{70}As were measured via the γ-ray lineshape method [8, 9], which takes advantage of the emission-point distribution of γ-rays emitted in flight from excited reaction residues. The Doppler reconstruction of these γ-rays assumes that they are emitted at the target position, but the lifetime of the excited states causes the emission to occur at some distance downstream of the target (about 1 mm for every 10 ps of flight time at a velocity $\beta = 0.34$). This causes the Doppler-reconstructed γ-ray photopeaks to acquire a slight shift in the peak position towards lower energies as well as a low-energy tail [8, 9]; an example of the asymmetry of the $8^+ \rightarrow 7^-$ γ-ray peak in ^{70}As can be

seen in the insets of Fig. 1. In order to maximize the sensitivity of the shape of the photopeaks to the lifetime, the Doppler correction was performed by measuring the velocity of each recoil event-by-event in the S800.

III. ANALYSIS

In order to extract lifetime information from the shape of the γ-ray distribution, simulated spectra were generated using a simulation package [10] which is based on the GEANT4 framework and has been modified to describe the current experimental setup, similarly to Ref. [9]. The simulation propagates the unreacted and reacted beams through the target material and models the reaction as a sudden, one-step process in which the initial projectile nucleus is instantaneously converted into the reaction residue of interest by the removal of the appropriate number of nucleons. To compensate for the possible bias that this reaction model may introduce, the simulation accepts three inputs which parametrize the energy and momentum imparted to the outgoing beam fragment by the reaction. These inputs are the fraction of the momentum lost due to the reaction mechanism (separate from the energy loss of the projectile or fragment as it propagates through the target material), the full width at half maximum of the momentum distribution of the outgoing fragment (a Gaussian shape is used for this profile), and finally an additional spread in the momentum which is modeled as a kick from the reaction in a random direction. With these parameters, the experimentally measured energy and momentum profile of the beam can be reproduced in the simulations. In addition, the spatial profile of the incoming beam is described in the simulations by providing the focus position of the incoming beam relative to the target position, as well as the spatial spread of the beam (which is assumed to be uniform) in both directions normal to the beam direction at the focus point. The beam direction is specified by providing the center of the distribution of angles in the dispersive and non-dispersive directions measured in the S800 spectrometer along with the width of these angular distributions, which are modeled as Gaussian. Providing these parameters allows the simulation to reproduce the spatial properties of the beam which are measured in the S800 spectrometer.

With the properties of the beam fixed in the simulation, simulated γ-ray spectra were generated. As with the experimental data, the simulation uses the target position for Doppler-shift correction but the lifetime that is input to the simulation allows the excited reaction residues to propagate some distance downstream of the target before decaying. This causes the simulated photopeaks to acquire the same asymmetric shape as those in the data, and therefore the simulated spectra can be compared to the data in order to determine the excited state lifetime. The simulated spectra were fit to the data using a χ^2 minimization procedure and the minimum was

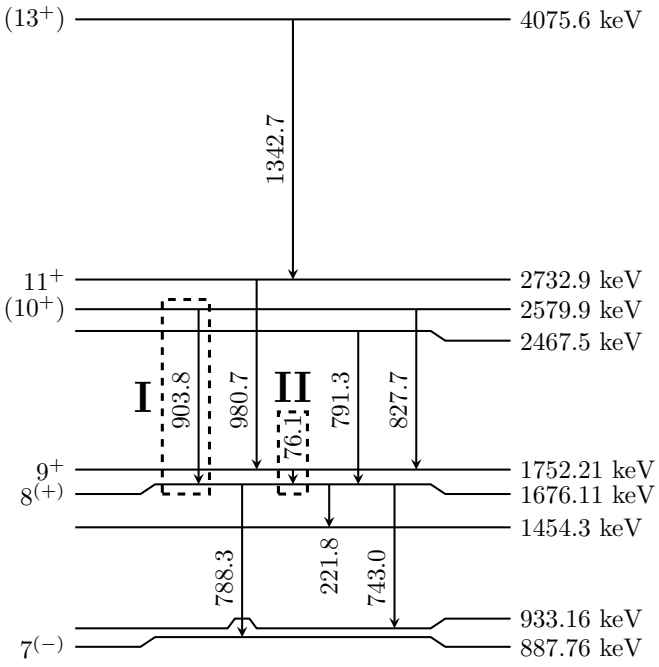

FIG. 2. A partial level scheme of ^{70}As indicating the levels which are relevant to this study, with the transitions labeled by the vertical text (in keV). The transitions which were used as gates to determine the lifetimes of the $8^{(+)}$ and 9^+ levels are indicated by the dashed boxes and are labeled I and II, respectively. Parentheses for tentative assignments are dropped in the text for simplicity. Data are from [15] except for the J^π of the (13^+) state, which is from [6].

used to extract the lifetime of the excited states. During the analysis, it was found that the backward ring of detectors was not sufficiently sensitive to the lineshape to extract a reliable lifetime. Therefore, only the forward ring was used to determine lifetimes, while the backward ring was used primarily to understand feeding patterns and to place gating conditions to generate $\gamma\gamma$ coincidence spectra.

The relationship between the 8^+ and 9^+ states which are of interest to this study and other nearby levels in ^{70}As are shown in Fig. 2. The 9^+ level deexcites to the 8^+ level via a 76.1 keV γ-ray, while the 8^+ deexcites mainly through a 788.3 keV transition to the 7^- level but also has a branch to the 933.16 keV state (13(2)% intensity relative to the 788.3 keV branch) and to the 1454.3 keV state (8(1)% intensity relative to the 788.3 keV branch). Figure 2 also shows that both the 8^+ and 9^+ levels may be fed by several other states. In particular, the 8^+ state may be fed directly by transitions from the 2467.5 keV state and the 2579.9 keV 10^+ state. The 9^+ state is also fed by the 2579.9 keV 10^+ state and by the 2732.9 keV 11^+ state. It should be noted that the J^π values and the γ-ray and level energies given in Fig. 2 and throughout this text are from [6, 15], as these values were not measured in this work. Levels below the 7^- state are not shown in the figure because the lifetime of this state is

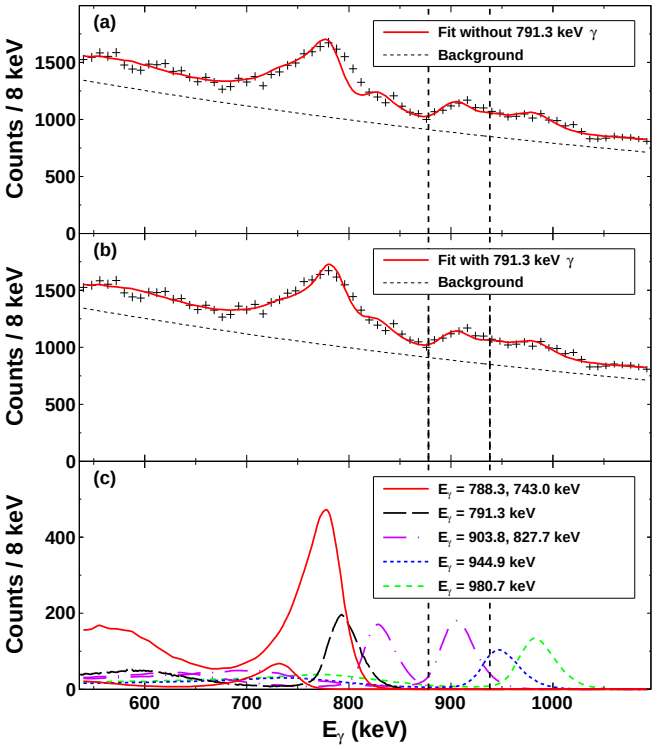

FIG. 3. (color online) Fits to the Doppler-corrected γ-ray singles spectrum obtained with the forward ring of detectors for ^{70}As, where the lifetime of the 8^+ state is fixed to 150 ps and only the amplitudes of the simulations are varied. The fit shown in (a) does not include the 791.3 keV γ-ray from the 2467.5 keV state, while (b) does contain the 791.3 keV γ-ray. Comparison between (a) and (b) makes it clear that the 791.3 keV γ-ray is necessary to reproduce the spectrum. Individual γ-rays included in the simulation in (b) can be seen in (c). The assumption for the exponential background is shown in (a) and (b) by the dashed curve. The vertical dashed lines indicate the area used to create gate I in Fig. 2 in order to generate the spectrum shown in Fig. 4(a).

very long (6.5 ns [6]), which causes the γ-rays from this state and the levels that it feeds to be so delayed that on average they are emitted long after the fragments have passed the SeGA detectors.

In order to understand the γ-ray singles spectrum from the forward ring of detectors, simulations were produced for the γ-rays depopulating the 1676.11 keV 8^+ level. As can be seen in Fig. 3, which shows a simulation assuming an 8^+ lifetime of 150 ps, small populations of higher-lying states can be observed above the 788.3 keV γ-ray depopulating the 8^+ level, and so simulations for the γ-rays from the states between the 9^+ and 13^+ levels shown in Fig. 2 were generated. For this initial fit, no account was taken of the lifetimes of these states or the feeding of the 8^+ state by the 9^+ state. A 944.9 keV γ-ray from the known 1026.3 keV level [15] (not shown in Fig. 2 because it is otherwise unrelated to the analysis) was also added, and an exponential background was fit across the region shown in Fig. 3. Feeding from the 2467.5 keV state had to be included in the simulations to account for a high-energy shoulder on the 8^+ 788.3 keV γ-ray peak. This level directly feeds the 8^+ state by a 791.3 keV γ-ray and cannot be resolved from the 788.3 keV $8^+ \rightarrow 7^-$ γ-ray. In addition, because it does not have a known lifetime, it may introduce a bias into the shape of the 788.3 keV γ-ray peak which would give an inaccurate lifetime determination.

Because of the near degeneracy of the 791.3 and 788.3 keV γ-rays, a different approach was necessary to determine the lifetime of the 8^+ state. Therefore, the lineshape method was used with $\gamma\gamma$ coincidence data. By fitting the coincidence spectra, feeding contributions to the 8^+ state lifetime can be eliminated by selecting a suitably fast decay as a gate. At the same time, by gating on a γ-ray that bypasses the 791.3 keV decay, the problem of having another unresolved transition beneath the $8^+ \rightarrow 7^-$ γ-ray is circumvented.

A coincidence spectrum for the 8^+ transition is shown in Fig. 4(a), which was created by placing a gate on the 903.8 keV transition depopulating the 2579.9 keV 10^+ state (gate I in Fig. 2). This decay connects directly to the 1676.11 keV 8^+ state, bypassing any other feeding contributions. The coincidence spectrum was then fit with simulations of the $8^+ \rightarrow 7^-$ decay and the lifetime of the state was extracted from the χ^2 distribution as $\tau_{8^+} = 80(28)$ ps, where the uncertainty is only statistical. While the lifetime of the (10^+) state is not known in ^{70}As, the analogous 10^+ state in ^{72}As has a $10^+ \rightarrow 8^+$ decay energy of 893.9 keV and a known lifetime of 1.10(20) ps [18]. By assuming the same decay strength in ^{70}As and ^{72}As, the lifetime of the 10^+ state in ^{70}As can be estimated to be 0.73 ps; this is less than 1% of the measured 8^+ state lifetime, and therefore it was neglected in the lifetime analysis. The best-fit result of the simulation to the data is shown in Fig. 4(a) by the solid line, and the inset shows the reduced χ^2 distribution. The background assumption is shown by the short-dashed line and was constrained by initially fitting over an energy range including the $8^+ \rightarrow 7^-$ transition plus background on either side, then the background was fixed and the lifetime was evaluated over a small region including only the peak area. A simulation which assumes a lifetime of 0 ps (long-dashed line) is also shown in Fig. 4(a) to demonstrate the sensitivity of the simulations to the lifetime.

Determination of the 9^+ lifetime was complicated by the fact that the 76.1 keV γ-ray that depopulates the 9^+ level is only visible in the backward ring which, as mentioned earlier, was found to be insufficiently sensitive to lifetime effects. In addition, as can be seen in Fig. 1(a), the 76.1 keV peak lies nearly on the detection threshold of the backward ring. Consequently, the low-energy tail of this peak may cross below the detector threshold, which can severely impede the accurate determination of the lifetime. Finally, the REC process referenced earlier makes the extraction of the lifetime from the γ-ray singles spectrum impractical. As stated in [16, 17], the energy of

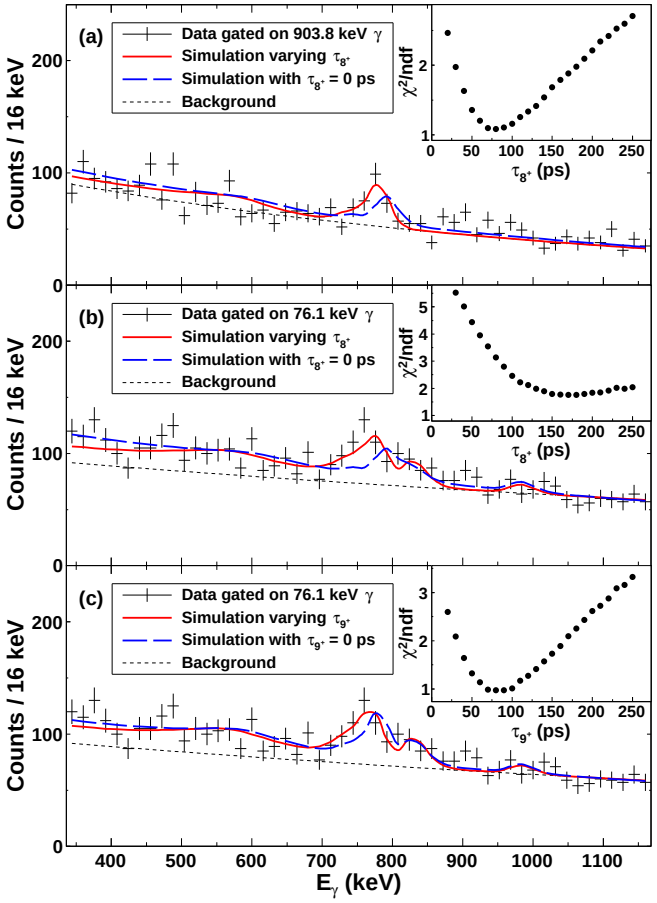

FIG. 4. (color online) Fits to the Doppler-corrected $\gamma\gamma$ coincidence data, with all panels showing the γ-rays in the forward ring. In each panel the solid curve is the best fit to the data while the short-dashed line indicates the assumption of the background. The long-dashed curve shows a simulation with a lifetime of 0 ps for comparison. Also shown in each panel is the χ^2 distribution for that fit. Panel (a) shows the fit to the experimental spectrum gated on the 903.8 keV γ-ray from the 10^+ state along with simulations in which the lifetime of the 8^+ state is varied. χ^2 analysis yields a lifetime of $\tau_{8^+} = 80(28)$ ps. Panel (b) shows the experimental data gated on the 76.1 keV γ-ray from the 9^+ state but attempts to fit this data with simulations which do not account for the 9^+ lifetime. These simulations fail to reproduce the experimental lineshape and result in a poor χ^2 distribution. Panel (c) shows the same data, but the simulations include feeding from the 9^+ state (with $\tau_{8^+} = 80$ ps fixed), as well as allowing for coincidence from above with the 827.7 keV and 980.7 keV γ-rays which populate the 9^+ state. This fit reproduces the lineshape of the 8^+ state, and χ^2 analysis yields a lifetime for the 9^+ state of $\tau_{9^+} = 85(30)$ ps.

the REC peak in the projectile frame (corresponding to the Doppler-reconstructed energy spectrum in Fig. 1) is the sum of the target electron kinetic energy in the beam frame and K electron binding energy in ^{70}As:

$$E_{REC} = \left(\frac{1}{\sqrt{1-\beta^2}} - 1 \right) m_e c^2 + E_b, \qquad (1)$$

where E_b is the electron binding energy and m_e is the electron mass. REC can have a cross-section of tens of barns [16, 17] and can happen either before or after the incoming ^{78}Rb beam reacts to form ^{70}As, and so the range of REC energies was calculated using velocities which correspond to ^{78}Rb as it enters the target ($\beta = 0.43$) and to ^{70}As as it exits the target ($\beta = 0.34$). Approximating the electron binding energy as that of a hydrogen-like atom of the appropriate species, the REC energy is calculated to range from $E_{REC} = 47$ keV to $E_{REC} = 74$ keV. The proximity of the 76.1 keV decay energy of the 9^+ state to the upper bound of the REC energy, combined with the lack of sensitivity and the threshold setting of the backward ring, made the determination of the lifetime of the 9^+ state also require $\gamma\gamma$ coincidence data.

To avoid the complications involved in measuring the 9^+ state lineshape directly, the lifetime of the 9^+ state was measured by analyzing its effect on the lineshape of the 8^+ state. A coincidence gate set on the 76.1 keV γ-ray from the 9^+ state (gate II in Fig. 2) resulted in the coincidence spectrum shown in Figs. 4(b) and (c), and simulations were performed to attempt to reproduce the 8^+ lineshape. Unlike the fit in Fig. 4(a), the 76.1 keV γ-ray can be in coincidence with the 827.7 keV γ-ray from the 10^+ state and the 980.7 keV γ-ray from the 11^+ state, and therefore these γ-rays were included in the simulations. In order to demonstrate the sensitivity of the data to the feeding lifetime of the 9^+ state, two sets of simulations were generated, one set which includes feeding from the 9^+ state and one set which does not. The solid curve in Fig. 4(b) shows simulations which do not include the feeding effects from the 9^+ state. These simulations cannot reproduce the lineshape of the experimental spectrum, even when the lifetime of the 8^+ state is increased to 160 ps. For comparison, the long-dashed line shows a simulation with an 8^+ lifetime of 0 ps to indicate the effect of increasing the lifetime. Finally, the inset shows that the reduced χ^2 distribution for this set of simulations does not find a good minimum. By contrast, Fig. 4(c) shows a fit to the same experimental spectrum as Fig. 4(b), but with simulations which properly account for the lifetime of the 9^+ state (the 8^+ lifetime was fixed to 80 ps as measured in this work). This fit provides a much better reproduction of the lineshape of the 788.3 keV γ-ray from the 8^+ state. The long-dashed curve shows a simulation with a 9^+ lifetime of 0 ps, further demonstrating the sensitivity of the lineshape to the lifetime in such a feeding scenario. The inset shows that the reduced χ^2 distribution has a clear minimum which yields a lifetime for the 9^+ state of $\tau_{9^+} = 85(30)$ ps, where the error is again only statistical. As in Fig. 4(a), the background in Figs. 4(b) and (c) is shown by the short-

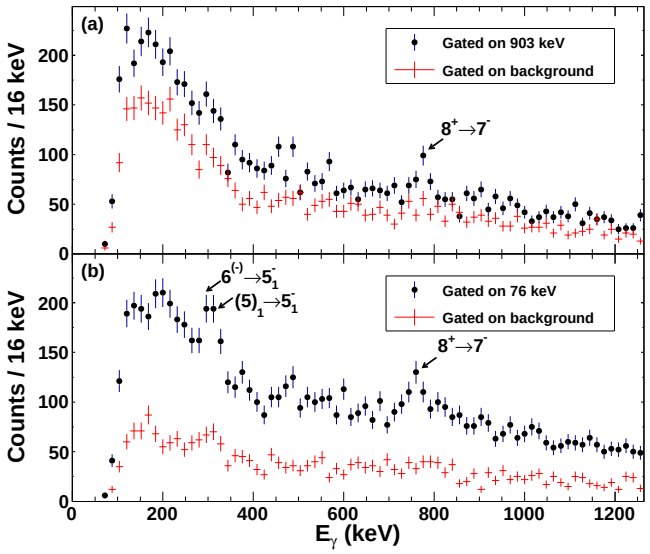

FIG. 5. (color online) (a) Doppler-corrected spectra from the forward ring generated for the gate on the 903.8 keV γ-ray from the 10^+ state and a gate of the same width placed at approximately 1200 keV in order to show the contribution from the background. There is a clear peak at 788.3 keV from the 8^+ state in the gate on the 903.8 keV γ-ray while there is no obvious contribution in the background gate. (b) Doppler-corrected spectra from the forward ring generated by placing a gate on the 76.1 keV γ-ray from the 9^+ state and a gate of the same width placed immediately above it in energy in order to show the background contribution. As in (a), there is a clear peak from the 8^+ state in the gate on the 76.1 keV γ-ray, but no evidence for a peak in the background spectrum. The peak at approximately 300 keV in the spectrum gated on 76.1 keV can be explained by coincidence with the 81.2 keV γ-ray from the $5_1^{(-)}$ state, which can be populated from the $6^{(-)}$ and $(5)_1$ states [15].

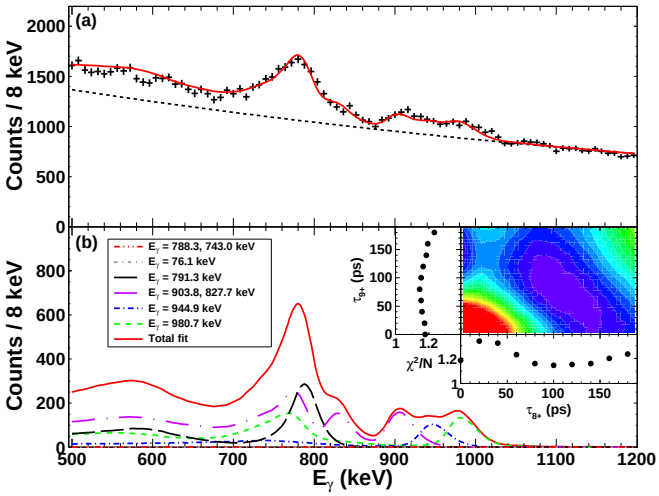

FIG. 6. (color online) (a) The fit to the Doppler-corrected γ-ray singles spectrum from the forward detector ring. The fit pictured was generated assuming the lifetimes $\tau_{8^+} = 100$ ps and $\tau_{9^+} = 80$ ps. The background was assumed to be exponential in shape and is indicated by the dashed line. (b) The individual components that went into the fit in (a). In contrast to Fig. 3, each component's feeding into the 8^+ state is included in the simulations, with the exception of the 944.9 keV γ-ray which does not feed the 8^+ state. Shown in the inset is the χ^2 surface generated by varying the lifetimes of the 8^+ and 9^+ states, with the projections of the minimum value for each gridline shown along each axis. To provide a sense of scale, the red area in the lower left of the χ^2 distribution corresponds to a value of $\chi^2/N \approx 2$, while the minimum value is approximately $\chi^2/N \approx 1.15$. Although the 1σ uncertainty limits lie outside the search area, the minimum can be clearly seen at $\tau_{8^+} \approx 100$ ps and $\tau_{9^+} \approx 80$ ps, in agreement with the results from the $\gamma\gamma$ coincidence fits.

dashed line, and was constrained in the same manner as it was for the lifetime of the 8^+ state.

In order to verify that the gates used to generate the $\gamma\gamma$ coincidence data are valid, $\gamma\gamma$ background spectra were generated and are shown in Fig. 5. Energy gates were placed on the γ-ray singles spectrum in locations where no coincidence with the 788.3 keV γ-ray from the 8^+ state was expected. For the gate on the 903.8 keV γ-ray from the 10^+ state, the presence of the 827.7 keV and 980.7 keV γ-rays from the 10^+ and 11^+ states, respectively, can contribute to the background gate, and so a higher energy background gate with the same width as the 903.8 keV gate was chosen at approximately 1200 keV to show the shape of background. The results of the 903.8 keV gate and the background gate can be seen in Fig. 5(a), which does not demonstrate a clear contribution to the 788.3 keV 8^+ state in the background spectrum. A similar procedure was followed to evaluate the background contribution for the 76.1 keV γ-ray from the 9^+ state. As mentioned earlier, the 76.1 keV γ-ray lies almost on the threshold of the SeGA detectors, and so a background gate was placed immediately above the 76.1 keV gate where no coincidence is expected with the 788.3 keV γ-ray from the 8^+ state. The gate on the 9^+ state along with the corresponding background gate can be seen in Fig. 5(b). It can be seen that there is a clear peak from the 8^+ state in the 76.1 keV gate, but evidently no contribution in the background gate. There is a broad peak at about 300 keV which may be from the $J^\pi = (5)_1$ and $6^{(-)}$ states around $860-900$ keV decaying to the $5_1^{(-)}$ state, both of which can be coincident with the 81.2 keV γ-ray from the $5_1^{(-)}$ state at 566.5 keV [15]. Background subtraction was not performed because the coincidence gates could not have background spectra generated by gating immediately above and below them, and therefore the shape of the background generated may not truly represent the background below the 8^+ state in Fig. 4. However, the absence of a clear peak in the background spectra in Fig. 5 demonstrates that the signals are coming from true coincidence events.

As an independent check that consistent results can be obtained, a fit to the γ-ray singles spectrum was performed in which the 8^+ and 9^+ lifetimes were var-

ied simultaneously and a search for a minimum in the χ^2 distribution was undertaken with respect to both of these variables. A full set of simulations including all feeding contributions to both the 8^+ and 9^+ states was generated and then fit to the data, resulting in the fit shown in Fig. 6(a) which assumes $\tau_{8^+} = 100$ ps and $\tau_{9^+} = 80$ ps. The individual components of the fit can be seen in Fig. 6(b), all of which include the correct feeding to the 8^+ state through either direct population or feeding from above (the 944.9 keV γ-ray excepted, since it comes from a state below the 8^+ state), thus ensuring that the intensity balance of the transitions incorporated in this fit is self-consistent. For these fits, the measured value of 1.1(3) ps was used for the lifetime of the 11^+ state [19], while the lifetime of the 10^+ state was assumed to be 0.73 ps based on the strength and γ-ray energy of the analogous decay in ^{72}As [18]. The lifetime of the 791.3 keV γ-ray from the 2467.5 keV state is unknown but was assumed to be comparable to the 10^+ state at about 1 ps. The components show that the population of the 8^+ state can be explained almost entirely by feeding from higher lying states, with the direct population of the 8^+ and 9^+ states being essentially zero. The inset in Fig. 6(b) shows the two-dimensional reduced χ^2 surface generated by searching for the best fit with respect to the 8^+ and 9^+ state lifetimes, as well as the projection of the minimum χ^2 value for a given lifetime onto the axes of the plot. These projections show that the minimum of the χ^2 surface lies in the vicinity of $\tau_{8^+} = 100$ ps and $\tau_{9^+} = 80$ ps. There is an apparent minimum in the χ^2 surface corresponding to $\tau_{8^+} = 0$ ps and $\tau_{9^+} = 160$ ps, but this result is clearly excluded by the $\gamma\gamma$ coincidence fit result for the 8^+ lifetime shown in Fig. 4(a). The sensitivity of the fit to the singles spectrum is lower than that of the $\gamma\gamma$ coincidence spectra and so the 1σ uncertainty limits lie outside of the search area, but the minimum of the two dimensional χ^2 surface is in agreement with the coincidence results.

Final uncertainty values for the lifetimes measured in this work were determined by examining systematic effects and accounting for the uncertainty of the 8^+ lifetime in the determination of the 9^+ lifetime. Systematic uncertainties were evaluated and found to be mostly due to the assumption of the background and to uncertainties in the geometry of the setup. The lifetimes of the 8^+ and 9^+ states were found to have a similar sensitivity to the background shape, with the 8^+ lifetime being slightly less sensitive (6.3% effect) than the 9^+ state lifetime (8.2% effect). The lifetimes were also found to have a small sensitivity to the range over which the background shape was fit, with the 8^+ sensitivity (1.1% effect) smaller than the 9^+ sensitivity (4.5% effect). The uncertainty due to the geometry of the experimental setup, in particular the relative positions of the target and the SeGA detectors, was evaluated and found to induce a 3% uncertainty in the lifetimes, consistent with Ref. [9] in which the same setup was used. Finally, the assumption of the lifetime of the (10^+) state can induce an additional systematic uncertainty. If this lifetime was increased by a factor of five, which would indicate a large change in the structure between ^{70}As and ^{72}As, it would change the lifetime of the 8^+ state by 3.4% and the lifetime of the 9^+ state by 4.4%. Added in quadrature, the systematic effects give an additional uncertainty of 7.8% to the 8^+ lifetime and 10.7% to the 9^+ lifetime. The uncertainty of the 8^+ lifetime was also propagated to the 9^+ lifetime uncertainty. Combining these uncertainties, the final lifetimes are given as $\tau_{8^+} = 80(29)$ ps and $\tau_{9^+} = 85(43)$ ps.

IV. DISCUSSION

In order to discuss the structure of the 8^+ and 9^+ states in ^{70}As, the lifetimes of the states measured in this work have been converted into reduced transition strengths. For the $8^+ \rightarrow 7^-$ transition, which has an E1 character with a small M2 admixture ($\delta = 0.017(13)$) [15], the transition strength is $B(E1) = 1.3(5) \times 10^{-5}$ e^2fm^2 or $1.2(4) \times 10^{-5}$ W.u. The $9^+ \rightarrow 8^+$ transition strength, which has an M1 character with a small E2 admixture ($\delta = 0.01(3)$) [15], is calculated to be $B(M1) = 1.5(8)$ μ_N^2 or 0.85(42) W.u. As shown in Fig. 2, the parities of the 8^+ and 7^- states are only given tentatively in [15], and therefore it is possible that different transition strengths should be calculated. If the parity of the $J = 8$ state is in fact negative, then the calculated transition strength should be $B(E1; 9^+ \rightarrow 8^-) = 1.5 \times 10^{-2}$ W.u. However, this exceeds the recommended upper limit for E1 transition strengths given in [20], which is 1.0×10^{-2} W.u. Since the recommended upper limit for M1 transitions is 3 W.u. [20], it is more likely that the $J = 8$ state is of positive parity. For the $J = 7$ state, a previous linear polarization measurement indicated that it is of negative parity [6]. Although the study reported this parity assignment as tentative, there is no experimental evidence to the contrary and so the parity of the $J = 7$ state is assumed to be negative in this work.

As discussed in the introduction, previous studies [5, 6] have suggested that the 8^+ state in ^{70}As should be composed primarily of the $\pi g_{9/2}\nu g_{9/2}$ configuration, and the strength of the $8^+ \rightarrow 7^-$ transition can give further insight into this assignment. The small strength of this E1 transition compared to those in the broader mass region [20] can be interpreted as indicating a hindrance of the decay. The 7^- state has been assigned to be composed mainly of the stretched configuration $\pi f_{5/2}\nu g_{9/2}$, based on the comparison of the measured half-life and magnetic dipole moment with theoretical calculations [6, 25]. For a pure E1 transition and states described by only the given shell model configurations, this decay should be forbidden by angular momentum conservation, as the proton must make a $\Delta J = 2$ transition from the $g_{9/2}$ orbital to the $f_{5/2}$ orbital. Small admixtures of other configurations can explain the existence of this transition, but the overall hindrance of the transition is consistent with the assignment of the 8^+

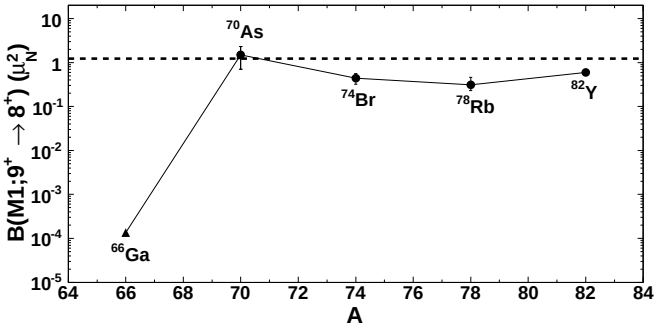

FIG. 7. $B(M1)$ values for several $9^+ \rightarrow 8^+$ transitions in nuclei in the vicinity of ^{70}As, along with a particle-vibration coupling model prediction indicated by the horizontal dashed line. The solid line is intended to emphasize the relative differences among the data points. The values for the selected nuclei with mass $A > 70$ are known, while the value for ^{66}Ga is tentative in that it is not certain whether the decay is of $E1$ or $M1$ character. If it is $M1$, then the drastic reduction from ^{70}As to ^{66}Ga suggests a sudden change in the nuclear structure. $B(M1)$ (or lifetime) data for other nuclei are taken from [21–24].

level to the $\pi g_{9/2}\nu g_{9/2}$ dominant configuration.

Information from analogous transitions can also help to characterize the structure of the 8^+ state in ^{70}As. The $8^+ \rightarrow 7^-$ transition in ^{72}As has a measured lifetime and has also been interpreted as originating from a $\pi g_{9/2}\nu g_{9/2}$ configuration [26] and ending in a $\pi f_{5/2}\nu g_{9/2}$ configuration [27]. The lifetime of this transition was measured to be 580(20) ps [28] and the E1 transition strength was deduced to be $B(E1) = 1.34(18) \times 10^{-5}$ e^2fm^2 or $1.22(16) \times 10^{-5}$ W.u. [26]. The close correspondence of the transition strength in ^{72}As with that found in ^{70}As supports the conclusion that the dominant coupling scheme of these states is the same.

The 9^+ state in ^{70}As has also been assigned a configuration of $\pi g_{9/2}\nu g_{9/2}$ based on the sum of the single-particle energies of the neighboring nuclei [6]. While the appropriate data are missing in neighboring As isotopes, the relevant lifetimes are known among the isotopes of other nearby elements [21–24]. Figure 7 shows the $B(M1)$ strengths of $9^+ \rightarrow 8^+$ transitions in nuclei along the α-chain that includes ^{70}As in which the 9^+ state is a member of the $\pi g_{9/2}\nu g_{9/2}$ configuration multiplet. As shown in the figure, the strength of the $9^+ \rightarrow 8^+$ transition in ^{70}As is comparable to the strength of the corresponding transitions in ^{74}Br, ^{78}Rb, and ^{82}Y, averaging between a factor of 2-3 times larger than in these nuclei. This similarity supports the assignment of the $\pi g_{9/2}\nu g_{9/2}$ configuration to the 9^+ state in ^{70}As.

Further insight into the nature of the $9^+ \rightarrow 8^+$ transition can be gained by using a model to calculate the expected $M1$ transition strength. The model chosen here has been used before to investigate the lower-lying states of ^{70}As [6] and is based on the coupling of two quasiparticles coupled to a vibrational core [29]. The form of the $B(M1)$ strength in this model (when $I_i > I_f$) is:

$$B(M1; I_i \rightarrow I_f) = \frac{3(j_p + j_n + I_i + 1)(j_p - j_n + I_i)(-j_p + j_n + I_i)(j_p + j_n - I_i + 1)}{4\pi I_i(2I_i + 1)} \left(\frac{\mu_p}{2j_p} - \frac{\mu_n}{2j_n} \right)^2 . \qquad (2)$$

With the odd-particle angular momenta $j_p = j_n = \frac{9}{2}$, $I_i = 9$, and following [29] in taking the quenching of the spin g-factors to be 0.6 such that

$$\frac{\mu_p}{2j_p} - \frac{\mu_n}{2j_n} = \frac{1}{2}\left\{ 1 + \frac{2.35}{2l_p + 1} + \frac{2.29}{2l_n + 1} \right\} \mu_N, \qquad (3)$$

the strength of the $9^+ \rightarrow 8^+$ transition calculated from the model is $B(M1) = 1.2\ \mu_N^2$ or 0.69 W.u. Compared to the measured strength of $B(M1) = 1.5(8)\ \mu_N^2$ or 0.85(42) W.u., the calculated value is consistent within the uncertainty and is shown in Fig. 7 as the horizontal dashed line. The sensitivity of the model can be evaluated by checking the result for the case of other spin scenarios. If the identification of the 8^+ and 9^+ states was reversed as is suggested to be the case in ^{68}As [30], the model would require that all I_i become I_f with the exception of the one in parentheses in the denominator [29]. In this case, the strength would be $B(M1) = 2.9\ \mu_N^2$ or 1.6 W.u., which is beyond the 1σ uncertainty limits of the experimentally measured value. However, the correct assignment of $J^\pi = 8^+$ and 9^+ spins gives better agreement between the calculation and experiment and supports the previous assignment of the $\pi g_{9/2}\nu g_{9/2}$ configuration to the 9^+ state.

Two final remarks about ^{70}As should be made before concluding. The first is to note the large difference in $B(M1; 9^+ \rightarrow 8^+)$ strength between ^{70}As and ^{66}Ga shown in Fig. 7. The point for the strength of the ^{66}Ga is tentative in that the parity of the $J = 8$ final state is not certain, and the knowledge of the character of the γ-ray connecting the two states is only that it is of dipole character [31]. If the parity of the state is positive and the γ-ray therefore of an M1 nature, then the $B(M1; 9^+ \rightarrow 8^+)$ value between ^{70}As and ^{66}Ga experiences a drastic decrease of four orders of magnitude. This sudden change in the transition strength compared to that between other nuclei in Fig. 7 indicates that while ^{70}As has a similar structure to the heavier nuclei along the α chain, there is a sudden change in the structure at ^{66}Ga and that ^{70}As lies on the edge of this change.

The second remark to be made is that a DSAM measurement of the lifetimes of the higher-lying 2732.9 keV 11^+ and 4075.6 keV (13^+) states has been performed previously and it was found that the $B(E2)$ strengths of these transitions indicated substantial collectivity [19]. Based on these results, it was concluded that the occupation of the $g_{9/2}$ orbital by both the odd proton and the odd neutron causes the shape of ^{70}As to become deformed in these high-spin states. Similarly, an interacting boson-fermion-fermion model calculation done for ^{72}As for the $\pi g_{9/2}\nu g_{9/2}$ multiplet of states found that it was necessary to assume a prolate-deformed core in order to reproduce the energy splitting of the levels in the multiplet [32]. In contrast, the results of this work do not necessarily require the core of ^{70}As to become deformed, as the strength of the $9^+ \rightarrow 8^+$ transition is fully consistent with a particle-vibration coupling description. A possible explanation for this contrasting behavior is that while core excitations are not required to produce the $\pi g_{9/2}\nu g_{9/2}$ coupling states up to spin 9^+ in ^{70}As, they are essential for the higher spin states above 9^+ and induce the deformation previously observed. A more complete understanding of the evolution of the core deformation as a function of spin in this nucleus could provide motivation for future investigations in ^{70}As.

In summary, we have measured the lifetimes of the 8^+ and 9^+ states in ^{70}As using the γ-ray lineshape method with $\gamma\gamma$ coincidence spectra. The calculated $B(E1; 8^+ \rightarrow 7^-)$ transition strength was found to indicate that the decay is a hindered transition, as well as being in good agreement with the corresponding decay in ^{72}As in which the 8^+ state has been assigned to the $\pi g_{9/2}\nu g_{9/2}$ configuration. The $B(M1; 9^+ \rightarrow 8^+)$ transition strength was found to agree well with the transition strength of decays between the 9^+ and 8^+ members of the $\pi g_{9/2}\nu g_{9/2}$ multiplet in neighboring nuclei and was also consistent with a particle-vibration coupling model calculation which assumed the same configuration. Based on these findings, the lifetime measurements in this work support previous studies which placed the 8^+ and 9^+ states in ^{70}As as members of the $\pi g_{9/2}\nu g_{9/2}$ configuration multiplet.

ACKNOWLEDGEMENTS

This work is supported by the National Science Foundation (NSF) under Grants No. PHY-0606007 and No. PHY-1102511, by the UK STFC, and by the Department of Energy (DOE) National Nuclear Security Administration under Award Number DE-NA0000979.

[1] W. Nazarewicz, J. Dudek, R. Bengtsson, T. Bengtsson, and I. Ragnarsson, Nucl. Phys. A **435**, 397 (1985).
[2] K. Heyde and J. L. Wood, Rev. Mod. Phys. **83**, 1467 (2011).
[3] M. Honma, T. Otsuka, T. Mizusaki, and M. Hjorth-Jensen, Phys. Rev. C **80**, 064323 (2009).
[4] K. Langanke, D. J. Dean, and W. Nazarewicz, Nucl. Phys. A **728**, 109 (2003).
[5] A. Filevich, M. Behar, G. García Bermúdez, M. A. J. Mariscotti, E. der Mateosian, and P. Thieberger, Nucl. Phys. A **309**, 285 (1978).
[6] T. Bădică, V. Cojocaru, D. Pantelică, I. Popescu, and N. Scîntei, Nucl. Phys. A **535**, 425 (1991).
[7] F. S. Stephens, R. M. Diamond, J. R. Leigh, T. Kammuri, and K. Nakai, Phys. Rev. Lett. **29**, 438 (1972).
[8] P. Doornenbal *et al.*, Nucl. Instr. and Meth. A **613**, 218 (2010).
[9] A. Lemasson *et al.*, Phys. Rev. C **85**, 041303 (2012).
[10] P. Adrich, D. Enderich, D. Miller, V. Moeller, R. P. Norris, K. Starosta, C. Vaman, P. Voss, and A. Dewald, Nucl. Instr. and Meth. A **598**, 454 (2009).
[11] A. Dewald, O. Möller, and P. Petkov, Prog. Part. Nucl. Phys. **67**, 786 (2012).
[12] D. J. Morrissey, B. M. Sherrill, M. Steiner, A. Stolz, and I. Wiedenhoever, Nucl. Instr. and Meth. B **204**, 90 (2003).
[13] D. Bazin, J. A. Caggiano, B. M. Sherrill, J. Yurkon, and A. Zeller, Nucl. Instr. and Meth. B **204**, 629 (2003).
[14] W. F. Mueller, J. A. Church, T. Glasmacher, D. Gutknecht, G. Hackman, P. G. Hansen, Z. Hu, K. L. Miller, and P. Quirin, Nucl. Instr. and Meth. A **466**, 492 (2001).
[15] J. K. Tuli, Nuclear Data Sheets **103**, 389 (2004).
[16] R. Anholt *et al.*, Phys. Rev. Lett. **53**, 234 (1984).
[17] Zs. Podolyák *et al.*, Nuclear Physics A **722**, 273 (2003).
[18] J. Döring, S. L. Tabor, J. W. Holcomb, T. D. Johnson, M. A. Riley, and P. C. Womble, Phys. Rev. C **49**, 2419 (1994).
[19] G. García Bermúdez, J. Döring, G. D. Johns, R. A. Kaye, M. A. Riley, S. L. Tabor, C. J. Gross, M. J. Brinkman, and H. Q. Jin, Phys. Rev. C **56**, 2869 (1997).
[20] P. M. Endt, At. Data and Nucl. Data Tables **23**, 547 (1979).
[21] T. Bădică, V. Cojocaru, D. Pantelică, I. Popescu, and R. Ion-Mihai, Hyperfine Interact. **36**, 171 (1987).
[22] G. García-Bermúdez, M. A. Cardona, A. Filevich, R. V. Ribas, H. Somacal, and L. Szybisz, Phys. Rev. C **59**, 1999 (1999).
[23] R. A. Kaye, L. A. Riley, G. Z. Solomon, S. L. Tabor, and P. Semmes, Phys. Rev. C **58**, 3228 (1998).
[24] S. D. Paul, H. C. Jain, S. Chattopadhyay, M. L. Jhingan, and J. A. Sheikh, Phys. Rev. C **51**, 2959 (1995).
[25] Zs. Podolyák, T. Fényes, and J. Timár, Nucl. Phys. A **584**, 60 (1995).
[26] J. Döring, D. Pantelică, A. Petrovici, B. R. S. Babu, J. H. Hamilton, J. Kormicki, Q. H. Lu, A. V. Ramayya, O. J. Tekyi-Mensah, and S. L. Tabor, Phys. Rev. C **57**, 97 (1998).
[27] D. Sohler, A. Algora, T. Fényes, J. Gulyás, S. Brant, and V. Paar, Nucl. Phys. A **604**, 25 (1996).
[28] D. Pantelica *et al.*, J. Phys. G **22**, 1013 (1996).
[29] M. Bogdanović *et al.*, Nucl. Phys. A **470**, 13 (1987).
[30] E. A. Stefanova *et al.*, Eur. Phys. J. A **24**, 1 (2005).
[31] E. Browne and J. K. Tuli, Nuclear Data Sheets **111**, 1093 (2010).
[32] D. Sohler, Zs. Podolyák, Zs. Dombrádi, J. Gulyás, A. Algora, S. Brant, V. Krstić, and V. Paar, Phys. Rev. C **59**, 1328 (1999).